

# COMMISSIONING THE MUON g-2 EXPERIMENT ELECTROSTATIC QUADRUPOLE SYSTEM\*

J. D. Crnkovic<sup>†</sup>, V. Tishchenko, Brookhaven National Laboratory, Upton, USA

J. M. Grange, Argonne National Laboratory, Argonne, USA

H. D. Sanders<sup>1</sup>, Applied Pulsed Power, Freeville, USA

<sup>1</sup>also at Sanders Pulsed Power LLC, Batavia, USA

N. H. Tran, Boston University, Boston, USA

A. T. Herrod<sup>2</sup>, The Cockcroft Institute, Warrington, UK

<sup>2</sup>also at University of Liverpool, Liverpool, UK

K. E. Badgley, H. Nguyen, E. Ramberg, Fermi National Accelerator Laboratory, Batavia, USA

E. Barlas Yucel, M. Yucel, Istanbul Technical University, Istanbul, Turkey

J. L. Holzbauer, W. Wu, University of Mississippi, University, USA

on behalf of the Muon g-2 Collaboration

## Abstract

The Fermilab Muon g-2 experiment aims to measure the muon anomaly with a precision of 140 parts-per-billion (ppb) – a fourfold improvement over the 540 ppb precision obtained by the BNL Muon g-2 experiment. These high precision experiments both require a very uniform muon storage ring magnetic field that precludes the use of vertical-focusing magnetic quadrupoles. The Fermilab Electrostatic Quadrupole System (EQS) is the refurbished and upgraded BNL EQS, where this overview describes the Fermilab EQS and its recent operations.

## INTRODUCTION

The magnetic ( $\vec{\mu}$ ) dipole moment for a fermion is given by

$$\vec{\mu} = g \frac{q}{2m} \vec{s},$$

where  $g$  is the dimensionless g-factor,  $q$  is charge,  $m$  is mass, and  $\vec{s}$  is spin. Dirac theory predicts  $g = 2$  for spin-1/2 point particles such as the muon, while Standard Model (SM) quantum field theory predicts  $g \neq 2$ . The deviation of  $g$  from 2 is given by the anomaly:  $a \equiv (g - 2)/2$ .

Magnetic dipole moment measurements [1–3] provide important tests of the SM, where the Brookhaven National Laboratory (BNL) [3] and Fermi National Accelerator Laboratory (Fermilab) [4] Muon g-2 experiments are part of a long history [2, 3] of measuring the muon anomaly ( $a_\mu$ ). The final BNL measurement [5] is

$$a_\mu = 116592091(54)(33) \times 10^{-11}, \quad (1)$$

where the first uncertainty in parentheses is statistical and the second is systematic. The uncertainties in Eq. (1) correspond

\* This document was prepared by the Muon g-2 Collaboration using the resources of the Fermi National Accelerator Laboratory (Fermilab), a U.S. Department of Energy, Office of Science, HEP User Facility. Fermilab is managed by Fermi Research Alliance, LLC (FRA), acting under Contract No. DE-AC02-07CH11359. This manuscript has been authored by employees of Brookhaven Science Associates, LLC under Contract No. DE-SC0012704 with the U.S. Department of Energy.

<sup>†</sup> jcrnkovic@bnl.gov

to a fractional statistical and systematic accuracy of 460 and 280 parts-per-billion (ppb) respectively, for a total precision of 540 ppb. There is a greater than  $3\sigma$  difference between the  $a_\mu$  measured value and SM prediction [5], which hints at the possibility of physics beyond the SM.

The Fermilab experiment can calculate [4]  $a_\mu$  from

$$a_\mu = \left( \frac{g_e m_\mu \omega_a}{2 m_e \langle \omega_p \rangle} \right) \left( \frac{\mu_e}{\mu_p} \right), \quad (2)$$

where  $g_e$  is the electron g-factor,  $m_\mu/m_e$  is the muon-electron mass ratio,  $\mu_e/\mu_p$  is the electron-proton magnetic moment ratio, and  $\omega_a$  is the muon anomalous spin precession frequency. The  $\langle \omega_p \rangle$  in Eq. (2) corresponds to the average magnetic field seen by the muons, where the field has been written in terms of the corresponding free proton Larmor frequency because pulsed nuclear magnetic resonance is used to measure the field. Values for  $g_e$ ,  $m_\mu/m_e$ , and  $\mu_e/\mu_p$  can be obtained from CODATA [6], and the experiment will measure  $\omega_a$  and  $\langle \omega_p \rangle$  to calculate the corresponding  $a_\mu$ .

The Fermilab Muon g-2 experiment is currently in the first physics data-taking run, where it has the goal [4] of measuring  $a_\mu$  with a final statistical and systematic precision each having a value of 100 ppb for a total precision of 140 ppb. The 100 ppb statistical uncertainty is for  $\omega_a$ , as the statistical uncertainty for  $\langle \omega_p \rangle$  is negligible, and the  $\omega_a$  and  $\langle \omega_p \rangle$  measurements are to each have a 70 ppb systematic accuracy.

## ELECTROSTATIC QUADRUPOLE SYSTEM

The experiment works by injecting a polarized muon beam from the Fermilab Muon Campus [7] into a circular storage ring and measuring the arrival time and energy of the decay positrons with 24 calorimeters [8, 9] placed uniformly around the inside of the ring. A modulation on top of the muon exponential decay is observed after applying a suitable

energy threshold cut ( $E_{th}$ ) to the decay positron counts ( $N$ ):

$$N(E_{th}, t) = N_0(E_{th}, t) e^{-t/\gamma\tau_\mu} \{1 - A(E_{th}, t) \cos[\omega_a t + \phi(E_{th}, t)]\}, \quad (3)$$

where  $t$  is time,  $N_0$  is normalization,  $A$  is asymmetry, and  $\phi$  is the so called “g-2 phase”.

The muon spin ( $\vec{s}$ ) precesses relative to the muon momentum ( $\vec{p}$ ) and can be written as [10],

$$\frac{d}{dt} (\vec{s} \cdot \hat{p}) = -\frac{q}{m} [\vec{s} - (\vec{s} \cdot \hat{p}) \hat{p}] \cdot \left\{ a_\mu \hat{p} \times \vec{B} + \left[ (1 + a_\mu) \frac{p}{mc\gamma} - \frac{mc\gamma}{p} \right] \frac{\vec{E}}{c} \right\}, \quad (4)$$

where  $\vec{B}$  is the storage ring magnetic field,  $\gamma$  is the Lorentz factor,  $c$  is the speed of light, and  $\vec{E}$  is the storage ring electric field. Equation (4) can be used to determine  $\omega_a$  which is found in Eqs. (2) and (3).

The so-called “lost muons” are muons lost from the storage ring beam during a measurement period [3, 4, 11, 12], and they lead to a correction factor in  $N_0$  from Eq. (3). Some of the muons from the initial lost muon population decay before being lost and the daughter positrons enter into the dataset used to fit for  $\omega_a$ . Muon losses occur throughout a measurement period, and therefore create a time dependent systematic effect. This essentially turns the spin g-2 phase at storage ring injection into a function of time if the lost muon population has a different average spin compared to the fully stored muon population. The  $\omega_a$  and g-2 phase parameters are strongly correlated in a fit to decay positron time spectra data which can lead to a pull on the  $\omega_a$  fit value.

The storage ring vertical magnetic field provides weak radial (horizontal)-focusing of the beam. The experiment requires a very uniform storage ring magnetic field to limit the systematic uncertainty on the  $\langle\omega_p\rangle$  measurement, which precludes the use of magnetic quadrupoles. Instead it operates with a muon beam at the so-called “magic momentum” of  $p = (mc) / \sqrt{a_\mu} \approx 3.094 \text{ GeV}/c$  and uses vertical-focusing electric quadrupoles in the storage ring. Use of magic momentum muons helps to limit the electric field systematic effect on the  $\omega_a$  measurement because the  $\vec{E}$  term vanishes in Eq. (4) for magic momentum muons.

The Electrostatic Quadrupole System (EQS) is turned on during a measurement period, but is otherwise turned off so as to reduce the rate of electrical sparking. It creates vertical-focusing for positive muons by applying positive voltage to the top and bottom plates along with weak horizontal-defocusing by applying negative voltage to the side plates. The vertical storage ring magnetic field more than compensates for the EQS horizontal-defocusing. Four pairs of long and short quadrupoles are placed around the storage ring to give a 4-fold symmetry, and in total span  $\sim 43\%$  of the ring. Each short quadrupole spans  $13^\circ$  of the storage ring, where the corresponding long quadrupole spans  $26^\circ$  and sits in the adjacent down-stream vacuum chamber. Figure 1 is a

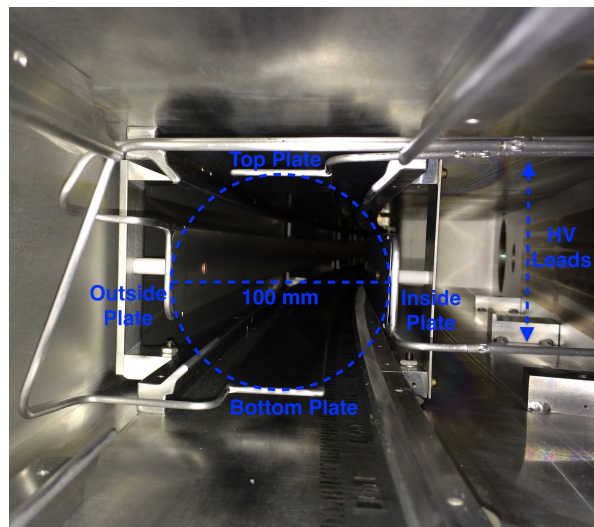


Figure 1: One end of a set of quadrupole plates and BNL EQS HV leads inside of a vacuum chamber. This picture was taken during Fermilab EQS R&D.

picture showing one end of a set of quadrupole plates and HV leads inside of a vacuum chamber.

There are 5 circular collimators that can be inserted into or retracted from the beam path, where these collimators create an effective 90 mm diameter circular aperture. Keeping the beam well within these collimators reduces the lost muons. Before a measurement period begins, the EQS is used to shift the beam down, radially outward on one side of the ring, and radially inward on the other side of the ring. After the shifted beam has been scraped against the collimators, it is adiabatically returned to the desired orbit (quadrupole plate voltages change with a nominal  $5 \mu\text{s}$  RC time constant).

## UPGRADES

The Fermilab Muon g-2 experiment EQS is the refurbished BNL Muon g-2 experiment EQS [13] that also includes several important upgrades. The muon beam passes through 2 quadrupole plates before being kicked onto the desired storage ring orbit. The BNL EQS used specially thinned aluminum for these plates to reduce muon scattering, while the Fermilab EQS uses aluminized mylar with an aluminum frame to further reduce scattering. The BNL EQS used thyatron based switches for generating high voltage (HV) pulses, while the Fermilab EQS instead uses solid state IGBT based switches. The IGBT switches allow for the quadrupole plates to be “connected” to the HV power supplies and capacitors over a full measurement period which helps to keep the plates charged.

The BNL experiment discovered that trapped low energy electrons, which are primarily from the ionization of residual gases, damage ceramic pieces on the vacuum side of the HV feedthroughs that transfer HV to the quadrupole plates inside of the vacuum system. Trapped electrons drift in the  $\vec{E} \times \vec{B}$  direction, following a path along the electrical leads that connect the plates to the feedthroughs. The Fermilab

Content from this work may be used under the terms of the CC BY 3.0 licence (© 2018). Any distribution of this work must maintain attribution to the author(s), title of the work, publisher, and DOI.

experiment uses EQS extensions to displace the feedthroughs toward the storage ring center and away from the vacuum chambers that sit in the storage ring magnet gap. The HV feedthroughs now sit in a low  $\vec{B}$  region that allows trapped electrons to escape to ground.

## OPERATIONS

Figure 2 shows the relative number of decay positrons, as measured by the Fermilab experiment real time Data Quality Monitoring (DQM) system, when beam scraping is turned off. Beam scraping can obscure individual betatron resonance effects, as the transition from scraping to storage voltages moves the beam through multiple resonances. A reduction in decay positrons is seen due to betatron resonances centered near the 13.0, 16.8, 18.8 and 21.2 kV EQS storage set-point voltages. An increase in lost muons due to betatron resonances is also measured with the calorimeters [12].

In Fig. 2 the decay positron calorimeter events pass the energy ( $E_e$ ) cut  $E_e > 1.8$  GeV and time after injection ( $t_i$ ) cut  $t_i > 21.25$   $\mu$ s, while all cluster calorimeter events pass the cuts  $E_e > 0.1$  GeV and  $t_i > 18.75$   $\mu$ s. The T0 counter is a scintillator detector used to measure the muon beam flux just before injection into the storage ring. The “Decay Positrons / T0 Integral” quantity provides a measure of storage efficiency for a given set of run conditions, while the “Decay Positrons / All Clusters” quantity provides a measure of  $\omega_a$  signal relative to calorimeter signal for “stored” muons. Both quantities are reduced by betatron resonances due to an increase in lost muons.

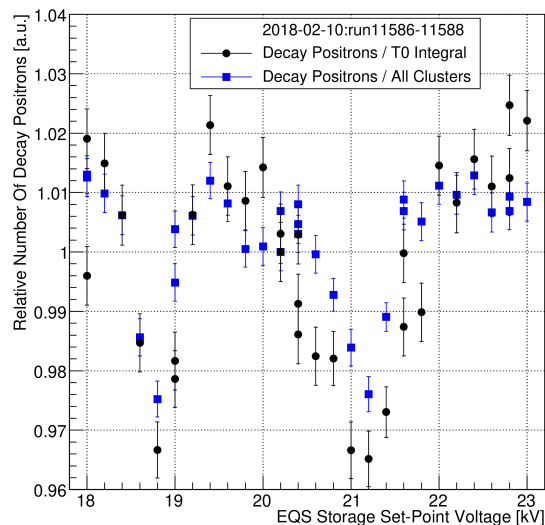
The experiment is currently in the first physics data-taking run, where EQS voltages for physics data-taking are chosen in the 15 to 21 kV range and are specifically selected to reduce resonance effects. Several sets of voltages are necessary, as the EQS does not always have stable operations due to spark recovery difficulties. The spark rate depends on conditions such as recent vacuum system exposure to atmosphere, extended EQS off-time, vacuum pressure, and EQS operating voltages. Collecting data at several different EQS operating voltages provides an opportunity for beam-dynamics related systematic checks. Finally, the EQS is used to scrape the beam for  $\sim 7$   $\mu$ s when taking physics data.

## CONCLUSION

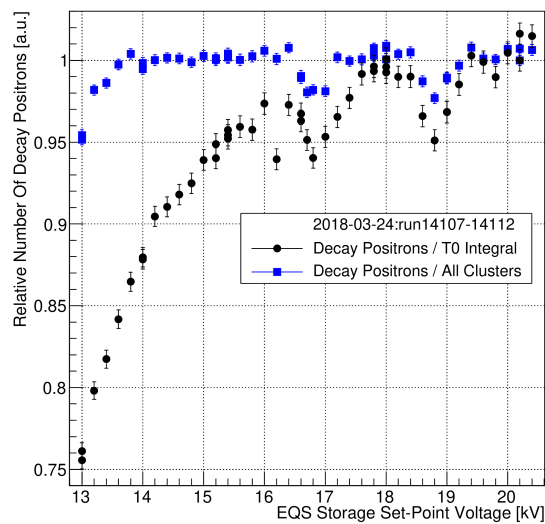
The Fermilab Muon g-2 experiment will measure  $a_\mu$  with unprecedented precision, where it is currently in the first physics data-taking run. The muon storage ring uses vertical-focusing electric quadrupoles, as magnetic quadrupoles are precluded due to the systematic uncertainty goal for  $\langle \omega_p \rangle$ . Several EQS operating voltages have been selected to avoid resonances, and the EQS is used to scrape the storage ring beam against collimators to reduce lost muons.

## ACKNOWLEDGMENT

The authors would like to thank William M. Morse for all of his advice and support in refurbishing, upgrading, and commissioning of the Fermilab EQS.



(a)



(b)

Figure 2: Typical relative number of decay positron scans as a function of EQS storage set-point voltage taken without scraping.

## REFERENCES

- [1] J. S. Schwinger, *Physical Review* **73**, 416 (1948). doi:10.1103/PhysRev.73.416
- [2] J. Bailey *et al.* [CERN-Mainz-Daresbury Collaboration], *Nucl. Phys. B* **150**, 1 (1979). doi:10.1016/0550-3213(79)90292-X
- [3] G. W. Bennett *et al.* [Muon g-2 Collaboration], *Phys. Rev. D* **73**, 072003 (2006) doi:10.1103/PhysRevD.73.072003 [hep-ex/0602035].
- [4] J. Grange *et al.* [Muon g-2 Collaboration], arXiv:1501.06858 [physics.ins-det].

- [5] C. Patrignani *et al.* (Particle Data Group), *Chin. Phys. C* **40**, 100001 (2016) and 2017 update.
- [6] P. J. Mohr *et al.*, *Rev. Mod. Phys.* **88**, no. 3, 035009 (2016) doi:10.1103/RevModPhys.88.035009 [arXiv:1507.07956 [physics.atom-ph]].
- [7] D. Stratakis *et al.*, *Phys. Rev. Accel. Beams* **20**, no. 11, 111003 (2017) doi:10.1103/PhysRevAccelBeams.20.111003 [arXiv:1803.00597 [physics.acc-ph]].
- [8] A. T. Fienberg *et al.*, *Nucl. Instrum. Meth. A* **783**, 12 (2015) doi:10.1016/j.nima.2015.02.028 [arXiv:1412.5525 [physics.ins-det]].
- [9] J. Kaspar *et al.*, *JINST* **12**, no. 01, P01009 (2017) doi:10.1088/1748-0221/12/01/P01009 [arXiv:1611.03180 [physics.ins-det]].
- [10] J. D. Jackson, *Classical Electrodynamics*, 3rd ed., (John Wiley & Sons, Inc., New York, 1999), pp. 561–565.
- [11] S. Ganguly *et al.*, *Proc. IPAC'17*, Copenhagen, Denmark, May 2017, paper WEPIK119, pp. 3230–3233.
- [12] S. Ganguly *et al.*, presented at IPAC'18, Vancouver, Canada, April 2018, paper THPAK139, this conference.
- [13] Y. K. Semertzidis *et al.*, *Nucl. Instrum. Meth. A* **503**, 458 (2003). doi:10.1016/S0168-9002(03)00999-9